Cumulant expansion of the periodic Anderson model in infinite dimensions

M E Foglio†§ and M S Figueira‡

† Instituto de Física 'Gleb Wataghin' Universidade Estadual de Campinas, UNICAMP 13083-970 Campinas, São Paulo, Brazil
‡ Instituto de Física, Universidade Federal Fluminense, UFF 24000-970 Niterói, Rio de Janeiro, Brazil

Abstract. The diagrammatic cumulant expansion for the periodic Anderson model with infinite Coulomb repulsion ($U = \infty$) is considered here for an hypercubic lattice of infinite dimension ($d = \infty$). The nearest neighbour hopping of the uncorrelated electrons is described exactly by a conduction band, while two different models of hybridization are treated as a perturbation. The same type of simplifications obtained by Metzner for the cumulant expansion of the Hubbard model in the limit of $d = \infty$, are also shown to be valid for the periodic Anderson model. The derivation of these properties had to be modified because of the exact treatment of the conduction band.

1. Introduction

The periodic Anderson model (PAM) gives a schematic description of very important systems with strongly correlated electrons, and there are several recent reviews on this subject [1]. The model consists of a lattice with two localized electronic states at each site, strongly correlated by a Coulomb repulsion U, plus a band of uncorrelated conduction electrons (c-electrons) that hybridize with the localized electrons (f-electrons). The cumulant expansion of the PAM discussed in this work is a perturbative expansion around the atomic limit, and is an extension [2] of the method originally employed by Hubbard [3] to study his well known model of correlated itinerant electrons [4]. He introduced operators $X_{j,ba} = |j, b\rangle\langle j, a|$, that transform the local state $|a\rangle$ at site j into the local state $|b\rangle$ at the same site, and developed a diagrammatic method that circumvents the fact that the X operators are neither fermions nor bosons. His work was the first application of the cumulant expansion to a quantum system of fermions [5] and has several desirable properties: it seems to be a natural extension of the usual diagrammatic techniques, it does not have excluded site problems in the lattice summations and it is possible to derive a linked-cluster expansion for the grand-canonical potential (see [2] for more details). At the same time, the use of X operators allows us to work in a subspace of the whole space of local states, that contains only the states that are relevant to the problem of interest. It therefore seems useful to understand this method better, and the main purpose of this paper is to study the properties of the cumulant expansion for the PAM in the limit of infinite spatial dimensions ($d \rightarrow \infty$).

Metzner and Vollhardt [6] have recently applied the limit $d \rightarrow \infty$ to strongly correlated fermion systems, providing non-trivial models of the Hubbard type that are substantially

§ Associate Member of ICTP, Trieste, Italy.

simpler to analyse. This development has stimulated many new works and we should mention the very successful dynamical mean field theory [7], that uses local properties of the self energy for $d \to \infty$ as a starting point. Several methods have been employed to study the PAM in this limit [8–11], the cumulant expansion of the Hubbard model was reconsidered by Metzner [12], showing that there is an important reduction in the number and type of cumulant diagrams that appear in the expansion when $d \to \infty$ in an hypercubic lattice. In the Hubbard model there is no hybridization and the hopping Hamiltonian is used as a perturbation, while the PAM is usually employed to model systems with a bandwidth much larger than the hybridization energies and it is then preferable to diagonalize the conduction band and use the hybridization Hamiltonian as a perturbation. It was then necessary to make substantial modifications to Metzner's derivation in order to apply it to the PAM when $d \to \infty$.

In the following sections two types of hybridization models are considered: the purely 'local' hybridization and the 'nearest-neighbour' (n.n.) one. In the n.n. hybridization there are electronic transitions between localized ('f') states at a site and conduction Wannier states at the nearest-neighbour sites, while in the local hybridization those transitions only occur at the same site. The same type of diagram cancellation obtained by Metzner for the Hubbard model is obtained for these two hybridization models in the PAM.

As the local hybridization between f and d or s electrons should vanish when the site has inversion symmetry, the n.n. hybridization discussed in this paper is more realistic than the local one, because it does not necessarily vanish for that type of site. The local approximation is usually employed because it makes the calculation simpler; and the changes introduced by an interatomic hybridization have been already discussed in the case of a diatomic-molecule model [13].

2. The hypercubic lattice

Let us consider free electrons in an hypercubic lattice of dimension d, described by a Hamiltonian [14]

$$H_c = \sum_{n,m,\sigma} t_{n,m} C^\dagger_{n,\sigma} C_{m,\sigma} \tag{2.1}$$

with translational invariance. The position of the site $n = (n_1, \ldots, n_d)$ is given by $R_n = \sum_{\alpha=1}^{d} e_\alpha n_\alpha$, where $|e_\alpha| = a$ is the lattice parameter and the n_j are integers. Only n.n. hopping shall be considered, so that $t_{n,m}$ is non-zero and equal to $-\bar{t}$ when the components m_α of m satisfy $m_\alpha = n_\alpha + \delta_{\alpha,\gamma}$ for $\gamma = 1, 2, \ldots, d$. Employing the Wannier transformation

$$C_{n,\sigma} = \frac{1}{\sqrt{N}} \sum_{k,\sigma} C_{k,\sigma} \exp[i k \cdot R_n] \tag{2.2}$$

with k satisfying cyclic boundary conditions, one obtains

$$H_c = \sum_{k,\sigma} E_k C^\dagger_{k,\sigma} C_{k,\sigma} \tag{2.3}$$

where

$$E_k = -2t \sum_{s=1}^{d} \cos(k_s a). \tag{2.4}$$

The electronic Green's functions (GF) for imaginary time are defined by [2]

$$G_\sigma(k,\tau) \equiv \langle (C_{k,\sigma}(\tau) C^\dagger_{k,\sigma})_+ \rangle \tag{2.5}$$

where $C_{k,\sigma}(\tau) \equiv \exp[H_c\tau]C_{k,\sigma}\exp[-H_c\tau]$ and the subindex $+$ in equation (2.5) is the usual chronological ordering of Fermi operators, with τ increasing to the left. To emphasize that the hybridization was not considered in these GF, they will be denoted with $G_\sigma^0(k,\tau)$, and after Fourier transformation in the imaginary time τ they are given by [15] $G_\sigma^0(k,\omega_v) = -(i\omega_v - E_k)^{-1}$. To obtain a finite average energy per site when $d \to \infty$, it is necessary to renormalize H_c, taking a finite t in the non-zero $t_{n,m} = -t/\sqrt{2d}$ (i.e. when n and m are n.n.). In that limit the energy density of states is given by [14]

$$\rho_d(E) = \frac{1}{\sqrt{2\pi t^2}} \exp\left[-\frac{E^2}{2t^2}\right] \tag{2.6}$$

and

$$\langle (E(k))^2 \rangle = t^2. \tag{2.7}$$

The exact solution of H_c is used in the present treatment of the PAM, employing the hybridization as a perturbation. To study the behaviour of the cumulant expansion in the limit $d \to \infty$, it is convenient to consider the direct space GF, given by

$$G_\sigma^0(R_{n,m}, \omega_v) \equiv \frac{1}{N} \sum_k G_\sigma^0(k,\omega_v) \exp[ik \cdot R_{n,m}] \tag{2.8}$$

where $R_{n,m} = R_n - R_m$, as well as its dependence with the minimum number p of n.n. jumps necessary to go from m to n. When the GF are obtained for large d using the hopping as a perturbation, one immediately shows that $G_\sigma^0(R_{n,m}, \omega_v) \simeq O|\theta|$, where $\theta = t/\sqrt{2d}$. A similar result is obtained for the 'exact' $G_\sigma^0(R_{n,m}, \omega_v)$ of equation (2.8), but the discussion will be postponed to a later section, in which a more general property will be shown.

3. The Hamiltonian of the PAM

The Hamiltonian of the whole system is

$$H = H_c + H_f + H_h \tag{3.1}$$

where H_c is the Hamiltonian of the c-electrons discussed in section 2. The second term $H_f = \sum_{j,\sigma} E_\sigma X_{j,\sigma\sigma}$ describes independent f-electrons, where a simple index j has been used to indicate the sites n. The last term is the hybridization Hamiltonian [2], giving the interaction between the c- and f-electrons:

$$H_h = \sum_{j,k,\sigma} (V_{j,k,\sigma} X_{j,0\sigma}^\dagger C_{k,\sigma} + V_{j,k,\sigma}^* C_{k,\sigma}^\dagger X_{j,0\sigma}). \tag{3.2}$$

The state space of the f-electrons, at a given site j, is spanned by four states: the vacuum state $|j, 0\rangle$, the two states $|j, \sigma\rangle$ of one f-electron with spin component σ and the state $|j, 2\rangle$ with two electrons of opposite spin. In the limit of infinite electronic repulsion ($U = \infty$) considered here, the state $|j, 2\rangle$ is always empty, and can be projected out of the space. The operator $X_{j,0\sigma}$ destroys the electron in state $|j, \sigma\rangle$ leaving the site in the vacuum state $|j, 0\rangle$ with energy $E_{j,0} = 0$, and its Hermitian conjugate $X_{j,0\sigma}^\dagger = X_{j,\sigma 0}$ reverses that process. The Hubbard operators $X_{j,ab}$ are not usually Fermi or Bose operators, and a product rule:

$$X_{j,ab} X_{j,cd} = \delta_{bc} X_{j,ad} \tag{3.3}$$

should be employed when the two operators are at the same site. For different sites one should first classify the operators in two families: $X_{j,ab}$ is of the 'Fermi type' when $|a\rangle$ and $|b\rangle$ differ by an odd number of Fermions, and it is of the 'Bose type' when they

differ by an even number of Fermions. At different sites, two X operators of the Fermi type anticommute, and they commute when at least one of them is of the Bose type. To complete the definition, the $X_{j,ab}$ should anticommute (commute) with the $C_{k,\sigma}^{\dagger}$ and $C_{k,\sigma}$ when they are of the Fermi type (Bose type). Sometimes it will be convenient to employ $X(\gamma)$ to describe the Hubbard operators, where $\gamma = (j, \alpha, u)$, and $\alpha = (b, a)$ gives the transition $|a\rangle \to |b\rangle$ that destroys one electron, i.e. with $|b\rangle$ having one electron less than $|a\rangle$ as in [15], and it is often convenient to abbreviate $(\gamma, \tau) = \ell$. The index u is then introduced to describe the inverse transition, so that $X(\gamma) = X_{j,\alpha}$ when $u = -$ and $X(\gamma) = X_{j,\alpha}^{\dagger}$ when $u = +$, and for the PAM with $U = \infty$ there are only two possible transitions $\alpha = (0, \sigma)$.

The grand canonical ensemble (GCE) of electrons is employed in this problem, and it is useful to introduce

$$\mathcal{H} = H - \mu \left(\sum_{k,\sigma} C_{k,\sigma}^{\dagger} C_{k,\sigma} + \sum_{j,a} \nu_a X_{j,aa} \right) \tag{3.4}$$

where ν_a is the number of electrons in state $|a\rangle$ and μ is the chemical potential. As usual $\mathcal{H}$ is split into

$$\mathcal{H} = \mathcal{H}_0 + H_{\mathrm{h}} \tag{3.5}$$

where H_{h} will be the perturbation Hamiltonian, and the exact and unperturbed averages of any operator A will be denoted respectively by $\langle A \rangle_{\mathcal{H}}$ and $\langle A \rangle$. It is also convenient to denote the exact or Heisenberg 'τ evolution' of any operator A with

$$\widehat{A}(\tau) = \exp(\mathcal{H}\tau) A \exp(-\mathcal{H}\tau) \tag{3.6}$$

and employ $A(\tau) = \exp(\mathcal{H}_0\tau) A \exp(-\mathcal{H}_0\tau)$ for the unperturbed case. It is convenient to use the expressions

$$\varepsilon_{j,a} = E_{j,a} - \nu_a \mu \qquad \text{and} \qquad \varepsilon_{k,\sigma} = E_{k,\sigma} - \mu \tag{3.7}$$

because the energies almost always appear in those combinations.

The c-electron GF employed in the cumulant expansion are:

$$G_{c,\sigma}^{o}(k,\omega) = -\frac{1}{i\omega - \varepsilon_{k,\sigma}} \tag{3.8}$$

where the subindex c was added to differentiate them from the unperturbed GF of the f-electron and

$$G_{f,\sigma}^{o}(\omega) = -\frac{D_{\sigma}^{0}}{i\omega - \varepsilon_{\sigma}} \tag{3.9}$$

where $D_{\sigma}^{0} = \langle X_{\sigma\sigma} \rangle + \langle X_{00} \rangle$. Although the $G_{f,\sigma}^{o}(\omega)$ is also a GF in the reciprocal space, it is independent of k because it corresponds to a band of zero width.

3.0.1. The two Hybridization models. The general hybridization coefficients are given by (cf [2, equation (2.3)])

$$V_{j,k,\sigma} = \frac{1}{\sqrt{N_s}} V_{\sigma}(k) \exp(ik \cdot R_j). \tag{3.10}$$

The hybridization is purely local when $V_{\sigma}(k) = V_{\sigma}^{0}$ is independent of k, because using the Wannier transformation (cf equation (2.2)) in equation (3.2) it follows that

$$H_{\mathrm{h}} = \sum_{j,\sigma} (V_{\sigma}^{0} X_{j,0\sigma}^{\dagger} C_{j,\sigma} + (V_{\sigma}^{0})^{*} C_{j,\sigma}^{\dagger} X_{j,0\sigma}). \tag{3.11}$$
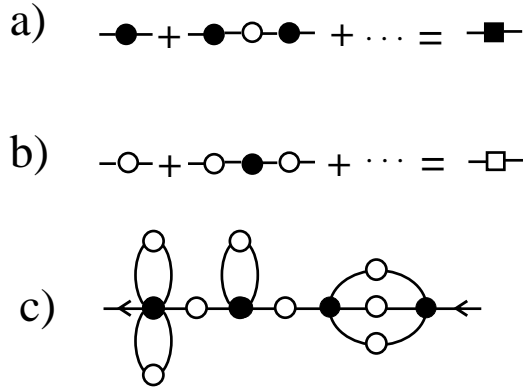
Figure 1. Typical cumulant diagrams for one-particle GF. (*a*) The diagrams of the CHA for the f-electron, represented by the closed square to the right. (*b*) As (*a*) but for the c-electrons, represented by an open square. (*c*) A more complicated diagram, with cumulants of fourth and sixth order.

The H_h that corresponds to n.n. hybridization is

$$H_h = \sum_{j,\delta,\sigma} (V_\sigma X^\dagger_{j+\delta,0\sigma} C_{j,\sigma} + (V_\sigma)^* C^\dagger_{j,\sigma} X_{j+\delta,0\sigma}) \tag{3.12}$$

where the vectors δ give the position of the d n.n. sites of the origin, and the corresponding $V_\sigma(\boldsymbol{k})$ is immediately obtained:

$$V_\sigma(\boldsymbol{k}) = 2V_\sigma \sum_{\alpha=1}^{d} \cos(k_\alpha a) = -\frac{V_\sigma}{t} E_{k,\sigma}. \tag{3.13}$$

3.1. The chain approximation

Some of the infinite diagrams that contribute to the exact GF $\langle(\hat{X}_{j,\alpha}(\tau)\hat{X}_{j',\alpha})_+\rangle_\mathcal{H}$ are shown in figure 1. The full circles (f-vertices) correspond to the cumulants of the f-electrons and the open ones (c-vertices) to those of the c-electrons. Each line reaching a vertex is associated with one of the X operators of the cumulant, and the free lines (i.e. those that do not join an open circle) correspond to the external X operators appearing in the exact GF. An explicit definition of the cumulants can be found in [2, 3, 15], and they can be calculated by employing a generalized Wick's theorem [15–17].

The first diagram in figure 1(*a*) corresponds to the simplest free propagator $\langle(X_{j,\alpha}(\tau)X_{j',\alpha'})_+\rangle$, and the second diagram in that figure has an open circle that corresponds to the conduction electron cumulant, equal to the free propagator $\langle(C_{k\sigma}(\tau)C^\dagger_{k\sigma})_+\rangle$. The interaction is represented by the lines (edges) joining two vertices and, because of the structure of the hybridization, they always join a c-vertex to an f-vertex; the number of edges in a diagram gives its order in the perturbation expansion.

Cumulants containing statistically independent operators are zero, and those appearing in the present formalism (with the hybridization as a perturbation) vanish unless they contain only X operators at the same site or only C or $C^\dagger$ operators with the same k and σ. The only non-zero c-cumulants are of second order, because the uncorrelated c-operators satisfy Wick's theorem. On the other hand, the f-vertices can have many legs, all corresponding

to X operators at the same site, like the fourth and sixth order cumulants appearing in the rather more complicated diagram shown in figure 1(c).

   All the infinite diagrams that contribute to the GF of the f-electron with cumulants of at most second order are shown in figure 1(a), and they define the 'chain approximation' (CHA) when all the other diagrams are neglected. The corresponding approximation for the GF of the c-electrons corresponds to the diagrams of figure 1(b). The diagrams of the CHA usually appear as part of more complicated diagrams, and it is then useful to analyse their behaviour when $d \rightarrow \infty$. In the CHA, the GF is given in frequency and k space by (cf [15, equation (3.10)])

$$G_{f,\sigma}(\boldsymbol{k}, \omega) = \frac{-(i\omega - \varepsilon_{k\sigma})D_\sigma^0}{(i\omega - \varepsilon_\sigma)(i\omega - \varepsilon_{k\sigma}) - |V(\boldsymbol{k})|^2 D_\sigma^0} \tag{3.14}$$

and it would be useful to transform it back to real space to show the dependence with the distance $\boldsymbol{R}_{i,j}$ between the two sites i and j, as was done in equation (2.8) for the conduction electrons. Because of the lattice translational invariance, it is enough to use the distance $\boldsymbol{R}_j$ of the site j to the origin, and characterize this site with an $\boldsymbol{n} = (n_1, \ldots, n_d)$, (cf section 2). The set of indices r with $n_r \neq 0$ will be denoted with $\{r\}_j$, while $s(j) = \sum_1^d n_s$ is the minimum number of n.n. jumps necessary to go from the origin to the site j. In both the local and the n.n. hybridization models, the $G_{f,\sigma}(\boldsymbol{k}, \omega)$ depends on k only through the $\varepsilon_{k\sigma} = E_{k\sigma} - \mu$, and for any given site j one can write

$$E_{k\sigma} = E_\sigma(\{r\}_j, \boldsymbol{k}) - \theta \sum_{s \in \{r\}_j} \cos(a k_s) \tag{3.15}$$

where

$$E_\sigma(\{r\}_j, \boldsymbol{k}) = -\theta \sum_{s \notin \{r\}_j} \cos(a k_s) \tag{3.16}$$

and $\theta = t/\sqrt{2d}$. Substituting this relation in equation (3.14) one can expand it in a power series of all the $\cos(a k_s)$ with $s \in \{r\}_j$ and then transform back to real space to obtain $G_{f,\sigma}(\boldsymbol{R}_j, \omega)$. Employing the relation

$$\sum_{k_s} \cos^m(k_s a) \exp(i n_s k_s a) = 0 \qquad \text{for } \boldsymbol{m} < \boldsymbol{n}_s \tag{3.17}$$

which is a consequence of the cyclic boundary conditions, it follows that

$$G_{f,\sigma}(\boldsymbol{R}_j, \omega) = O|(2d)^{-s(j)/2}|. \tag{3.18}$$

The GF for the conduction electrons in the CHA, corresponding to the diagrams in figure 1(b), is given by:

$$G_{c,\sigma}(\boldsymbol{k}, \omega) = \frac{-(i\omega - \varepsilon_\sigma)}{(i\omega - \varepsilon_\sigma)(i\omega - \varepsilon_{k\sigma}) - |V(\boldsymbol{k})|^2 D_\sigma^0} \tag{3.19}$$

and employing the same derivation used above for the f-electrons it follows that $G_{c,\sigma}(\boldsymbol{R}_j, \omega) = O|(2d)^{-s(j)/2}|$. The same relation is obtained in the absence of hybridization, as stated at the end of section 2 for $G_\sigma^0(\boldsymbol{R}_{n,m}, \omega_v)$.

   To close this section let us emphasize that the present expansion employs H_h as a perturbation, and that the exact solution of the conduction problem in the absence of hybridization is included in the zeroth order Hamiltonian. The contribution to the GF joining two sites separated by $s(j)$ n.n. jumps, that is of order $|(2d)^{-s(j)/2}|$, includes then contributions of any order in the H_c. It is because of this difference that the derivation of Metzner [12] for the Hubbard model had to be modified for the present problem.

   All the contributions of H_c would disappear in the case of a band with zero width, but the electronic wavefunctions would still be extended for the model with n.n. hybridization.
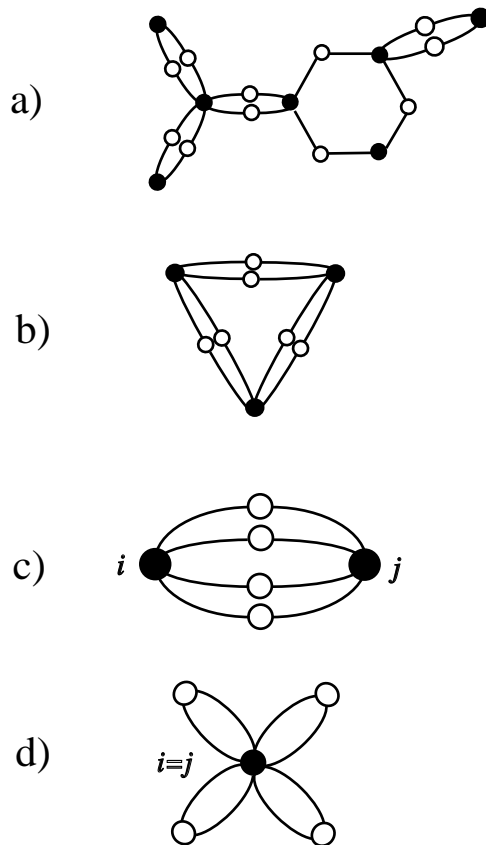
Figure 2. Examples of relevant topologies in the limit $d \to \infty$. (*a*) f.t.p.r.: any pair of vertices can be separated by cutting two edges. Note that all pairs of loops have at most one vertex in common. (*b*) The diagram is not f.t.p.r. (*c*) The topology of the diagram and that of the embedding are the same when $i \neq j$. (*d*) The embedding topology that corresponds to the diagram in (*c*) when $i = j$.

4. The contribution of diagrams for infinite dimension

In this section it will be shown that the only diagrams that remain in the limit $d \to \infty$ are those that are topologically 'fully two-particle reducible' (f.t.p.r.). These diagrams are defined as those in which any pair of vertices can be separated by cutting one or two edges [18], and are 'topologies constructed by linking polygons' [12]. Two points should be made here: the first is that two different polygons (also called loops or rings in what follows) can have at most one vertex in common in the f.t.p.r. topology (see figure 2(*a*) and (*b*)). The second point, already stressed by Metzner for the Hubbard model, [12] is that the topology of a diagram can be different from those of its possible embeddings in the lattice, because in the cumulant expansions there is no excluded site restriction in the lattice sums [2], and two different vertices of a diagram can occupy the same site (see figure 2(*c*) and (*d*). The property stated above refers to the topology of the embeddings, and in the sum of contributions of diagrams that are not f.t.p.r. there may be terms that give non-zero contributions because they correspond to a f.t.p.r. topology of the embedding: the diagram in figure 2(*c*) could contribute when $j = i$, because the topology of its embedding, given by figure 2(*d*), is f.t.p.r.
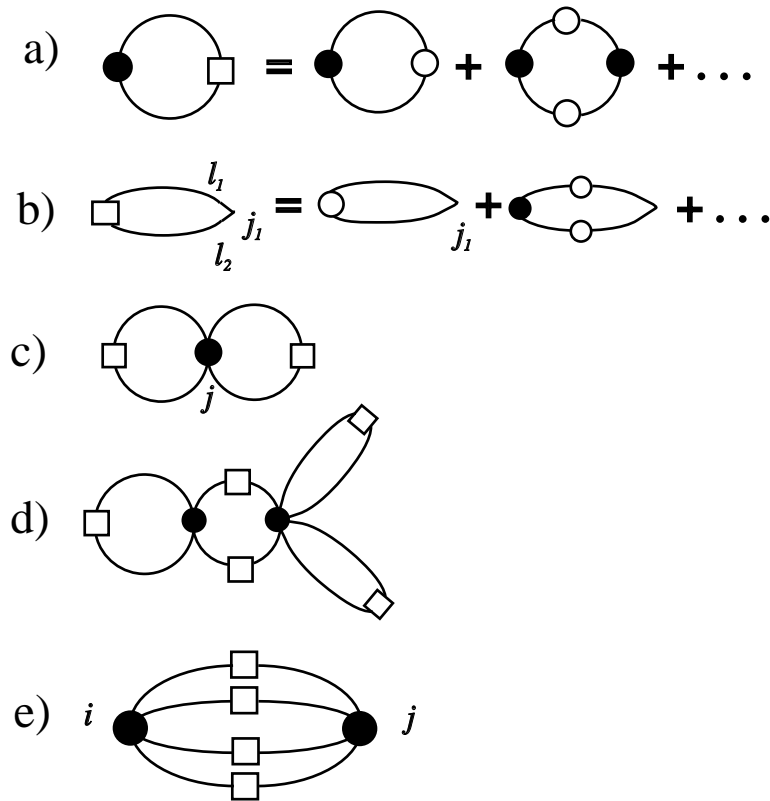
Figure 3. (a) The sum of all the simple loops of any length. (b) Diagrams of an insertion with contribution $S_2^0(j_1; \ell_1, \ell_2)$, obtained by fixing the site j_1 and the parameters ℓ_1, ℓ_2 of one local f-vertex (that is considered external) of the diagrams in (a). The full circle in these vertices, corresponding to the cumulant $M_2^0(j_1; \ell_1, \ell_2)$, is removed from the diagrams and is replaced by 1 in $S_2^0(j_1; \ell_1, \ell_2)$. ($c$) A f.t.p.r diagram obtained by joining two simple loops at an f-vertex. (d) Family of four linked loops that give a f.t.p.r diagram. (e) Family of diagrams obtained by linking two loops at two different f-vertices: it is not f.t.p.r.

To prove this property it is necessary to modify the derivation given by Metzner for the Hubbard model, for the same reasons given in section 3.1 for the GF dependence on $s(i)$. The proof of this property is given in the following two subsections, and it can be summarized as follows. Consider first the diagram in figure 3(a), that corresponds to the sum of loops with all possible lengths. All the embeddings of these diagrams are f.t.p.r., and they give a non-zero contribution to the calculation of the free energy. As a second step, one can consider diagrams like those in figures 3(c) and (d), obtained by linking loops of any length at different f-vertices. One could obtain all these diagrams by a procedure similar to the vertex renormalization [2, 5, 12], with the difference that only insertions of a rather special type are considered. All these diagrams, as well as their embeddings, are f.t.p.r. and a finite contribution of all of them is expected. The next step is to consider diagrams that are not f.t.p.r. like the one shown in figure 3(e), that can be obtained by joining two loops (as in figure 3(a)) at two different f-vertices. If the family in figure 3(a) gives a finite contribution, one can show that all the contributions to the diagram in figure 3(e) will vanish when the topology of the embedding coincides with that of the diagram, i.e.

when the embedding is not f.t.p.r., as would happen when $i \neq j$. In the special case of $i = j$, (cf figures 2(c) and (d) for a special case of this situation) the embedding is f.t.p.r. and the diagram contribution does not necessarily vanish. Of the two sums over the lattice sites i and j, only one over $i = j$ remains in the limit $d \rightarrow \infty$, and this simplifies the calculation of this diagram. In particular, the restriction that in reciprocal space there must be conservation of k at each vertex is removed [6, 14], leaving only a single conservation of k for all the edges joining the collapsed vertices: this makes the calculation of the diagram much simpler in the limit $d \rightarrow \infty$.

4.1. The f.t.p.r. diagrams

To prove that the contribution of a f.t.p.r. diagram can be finite, let us consider the family of diagrams represented in figure 3(a). Their contribution does not vanish and can be expressed as

$$\sum_{j_1} \int d\ell_1 \int d\ell_2 \, S_2^0(j_1; \ell_1, \ell_2) M_2^0(j_1; \ell_1, \ell_2) \tag{4.1}$$

where

$$M_2^0(j_1; \ell_1, \ell_2) = \langle (X(\ell_1)X(\ell_2))_+ \rangle_c \tag{4.2}$$

is a local cumulant [2] and $\int d\ell_s = \sum_{\alpha_s} \sum_{u_s} \int_0^\beta d\tau_s$. The abbreviations $s \equiv \ell_s$ and $\int ds \equiv \int d\ell_s$ will be used when there is no possibility of confusion. The symbol $S_2^0(j_1; \ell_1, \ell_2) \equiv S_2^0(j_1; 1, 2)$ corresponds closely to the 'self-field' [5] $S_m(j_1; \ell_1, \ell_2, \ldots, \ell_m) \equiv S_m(j_1; 1, 2, \ldots, m)$, that was employed in [15] to renormalize vertices, but it gives only 'insertions' obtained from simple loops of any length, as represented by the diagrams in figure 3(b); by definition, all the ℓ_s correspond to the same site, indicated by j_1. The notation $M_2^0(j_1; \ell_1, \ell_2) \equiv M_2^0(j_1; 1, 2)$ has the same meaning, and reflects the fact that this cumulant is zero unless $j_1 = j_2$ because $X(\ell_1)$ and $X(\ell_2)$ are statistically independent in the unperturbed system when $j_1 \neq j_2$. Note that $S_2^0(j_1; \ell_1, \ell_2)$ depends explicitly on the parameters $j_1; \ell_1, \ell_2$ (where ℓ_i represents $j_i, u_i, \alpha_i = (0, \sigma_i)$ for $i = 1, 2$) through the two hybridization constants $V_{j,k,\sigma}$ associated with the edges joining the insertion vertex.

To consider the addition of a simple loop to any f-vertex of a diagram, it is convenient to consider first the simplest possible case, shown in figure 3(c): its contribution is obtained by substituting the cumulant $M_2^0(j_1; 1, 2)$ in equation (4.1) by

$$\int d3 \int d4 \, M_4^0(j_1; 1, 2, 3, 4) S_2^0(j_1; 3, 4). \tag{4.3}$$

When the loop is added to a site j_1 that is already joined by n edges, the corresponding cumulant $M_m^0(j_1; 1, 2, \ldots, m)$ suffers a similar substitution. Repeated application of this procedure at all f vertices gives all the possible f.t.p.r diagrams, and as the cumulants are independent of the lattice dimension d and of the site j, this procedure should not affect the order of the contribution with respect to d. The simple loops of figure 3(a) give a finite contribution, so that the contribution of any f.t.p.r diagrams is then of $O(|d|^0)$.

A similar type of procedure can be applied to the CHA diagrams of the one-particle GF, by successive decoration of the f-vertices with any number of insertions corresponding to the $S_2^0(j_1; \ell_1, \ell_2)$ discussed above. It is then clear that these diagrams will still be f.t.p.r., and that the corresponding GF joining two sites separated by s n.n. jumps will be of $O|(2d)^{-s/2}|$, as shown in section 3 for the CHA.
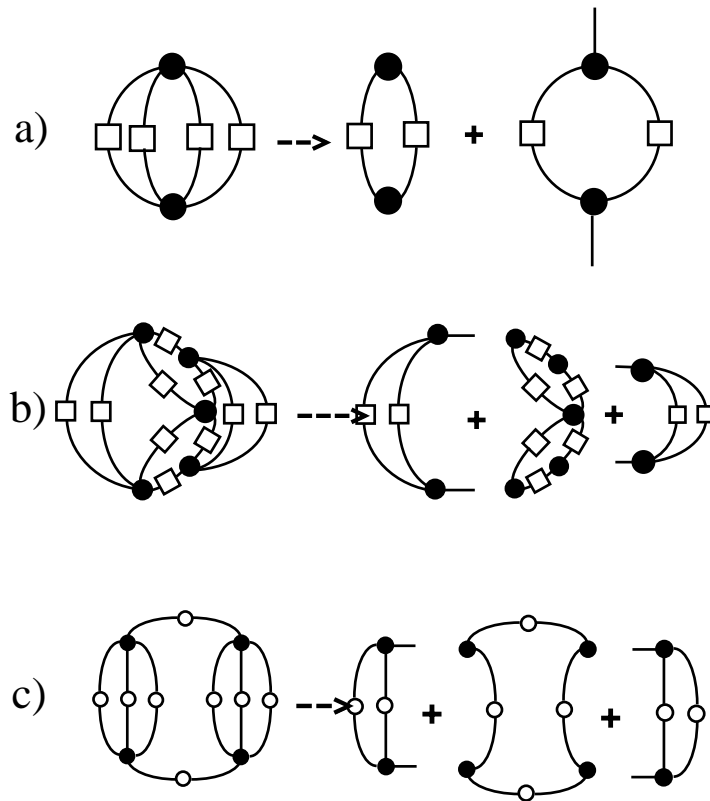
Figure 4. Three examples of separation of a mother vacuum diagram into several daughter diagrams. (*a*) Simplest case of separation with two common vertices. (*b*), (*c*) Separation in three daughter diagrams with a total of four shared vertices.

4.2. The diagrams that are not f.t.p.r.

To analyse the diagrams that are not f.t.p.r., consider any one of them as a 'mother' diagram, and split it into two or more f.t.p.r linked 'daughter' diagrams without any edges in common but such that any of them has at least two vertices in common with another daughter diagram, as well as two edges arriving at each of the common vertices. It is clear that any pair of vertices that are common to two daughter diagrams cannot be separated in the mother diagram by cutting one or two edges, and one says that they are not 'two-particle reducible' (t.p.r.).

From all the daughter diagrams choose one as a vacuum diagram and transform the remaining ones into GF by adding external lines of the Bose type (as indicated in appendix A) to all the vertices that each of them had in common with any other daughter diagram in the mother diagram. Three examples of this procedure are given in figure 4.

Consider now the real space calculation of the contribution of the daughter diagrams. In appendix A it is shown that by joining one daughter GF to another diagram and fixing the position of the common vertices, one obtains the order of the contribution of the resulting diagram as the product of those of the building diagrams. In appendix B it is shown that unless all the external f-vertices of one daughter GF coincide at the same lattice site, the corresponding contribution is of $O|(\theta)^p|$ with $p \geqslant 1$, where $\theta = t/\sqrt{2d}$. Taking now the
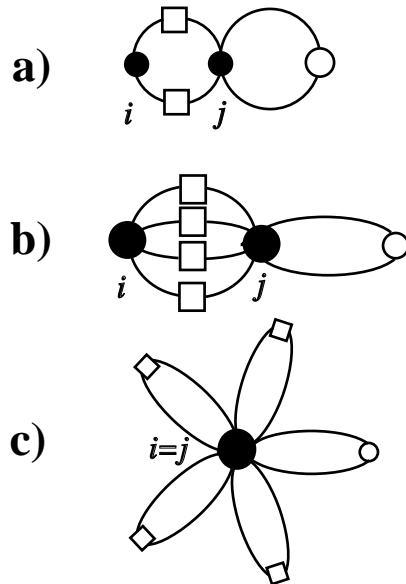
Figure 5. (*a*) A family of f.t.p.r diagrams that give a finite contribution for large *d*. (*b*) Family of diagrams obtained by joining pairs of f.t.p.r diagrams in two common vertices; the diagrams are not f.t.p.r. (*c*) The f.t.p.r topology of the embedding of (*b*) when $i = j$. Note that the diagram contribution is calculated with the diagram (*b*) and not with (*c*), but replacing the two independent summations over i and j by a single one over $i = j$.

only daughter vacuum diagram and adding successively all the other daughter GF diagrams, the total contribution for given positions of all the GF external vertices will then be $O|(\theta)^p|$ with $p \geqslant 1$, unless all the external vertices of each daughter GF coincide at the same lattice site, that can be different for different daughter GF. A typical example of this type of diagram is given in figure 5(*b*), while figure 5(*c*) shows the corresponding f.t.p.r. topology of the embedding when the vertices that are not t.p.r. in the diagram are at the same lattice site.

It is then clear that in the sum over the vertices that are common to all the daughter diagrams, each of the terms will be at best of $O|\theta|$, and would vanish in the limit $d \to \infty$, unless all the external vertices of each daughter diagram are at the same lattice site, that can be different for different daughter diagrams. One can conclude that the contribution of the mother diagram would vanish when any pair of vertices i and j that are not t.p.r. occupy different lattice sites, because in that case, it is always possible to separate from the mother diagram a daughter GF that has i and j in common with the rest of the diagram. In that case, only a sum over $i = j$ should remain from the unrestricted sum over i and j, and those two vertices then become t.p.r. in the embedding of the diagram (this is illustrated in figures 5(*b*) and (*c*)). This reduction of the terms that contribute to the lattice summations has already been described, and called 'collapse of vertices', in the study of the U-perturbation theory in high dimensions [14, 18]: this property will be given the same name in this work.

One important point to notice, is that the collapse of vertices occurs only in the embedding of the diagram, and that the rules for calculating the contribution should be applied to the original diagram (i.e. it would be the diagram of figure 5(*b*) in the examples given) and not to the collapsed diagram of the embedding (i.e. the diagram in figure 5(*c*)).

As in the collapse of i and j the two independent lattice summations over the vertices i and j are replaced by a single lattice summation over $i = j$, it is easy to see from the derivation of the contribution rules in reciprocal space (cf [2, section III D]) that the two independent momentum conservation at each of the two collapsed vertices becomes a single conservation of the wavevectors corresponding to all the internal edges joining them. When all the pairs of vertices that are not t.p.r. have been collapsed, one can see that at every vertex of the embedding of a vacuum or one-particle GF diagram, all the edges can be arranged in pairs with momentum k_s and $-k_s$ respectively (cf figure 5(c) as a typical example) It then follows that the momentum conservation at the collapsed vertices are automatically satisfied, and most of the usual restraints on the momentum integration disappear in the limit $d \to \infty$.

5. Summary and conclusions

The cumulant expansion of the PAM [2] was considered in the limit of infinite spatial dimensions ($d \to \infty$) for two types of hybridization models: the purely 'local' hybridization and the 'n.n.' one. As the systems usually described by the PAM have a bandwidth much larger than the hybridization energies, the unperturbed Hamiltonian is chosen to include the exact solution of the c-band electrons in the absence of hybridization. It is then necessary to modify the derivation employed by Metzner [12] for the cumulant expansion of the Hubbard model, in which the hopping Hamiltonian is used as a perturbation. The basic result presented here is that in spite of this change the PAM shows, for the two hybridization models considered, the same type of simplifications that occur in the diagrammatic cumulant expansion of the Hubbard model when $d \to \infty$.

Only the linked diagrams contribute to the general cumulant expansion, and there is a vertex collapse when $d \to \infty$ for those diagrams that are not f.t.p.r. A diagram is not f.t.p.r. when at least two vertices i and j can not be separated by cutting only one or two edges of the diagram, and their collapse means that from the two independent summations over i and j that are necessary to calculate their contribution, only a summation over $i = j$ remains. The topology of the embedding is different from that of the diagram itself when $i = j$, and the collapse is repeated until the topology of the embedding becomes f.t.p.r. One important point to note is that, after the collapse of vertices, the rules for calculating the contribution should be applied to the original diagram and not to the collapsed diagram of the embedding.

When the two independent summations over i and j of the diagram become a single summation over $i = j$ because the two vertices i and j collapse, the two separate conservations of k at these vertices become a single conservation of the k corresponding to all the edges joining both i and j. As a consequence, most of the usual restraints on the momentum integration disappear in the limit $d \to \infty$, and the calculation of many diagrams is very much simplified by this change. One should note that the vertex collapse does not alter the calculation over frequencies, which keep their conservation at all the diagram vertices, even when $d \to \infty$.

Employing the cumulant expansion, Metzner has shown [12] that the single-particle properties of the Hubbard model in the limit $d \to \infty$, can be described as that of independent electrons 'hopping between dressed atoms characterized by an effective GF' [19]. A similar derivation can be employed for the PAM, and the exact one-electron GF is given by the family of diagrams in figure 1(a), but using an effective cumulant $M_{2,\sigma}^{\text{eff}}(\omega)$ for the f-electron vertices instead of the bare one $M_{2,\sigma}^0(\omega)$. The effective cumulant $M_{2,\sigma}^{\text{eff}}(\omega)$ is given by the

contribution of all the diagrams of $G_\sigma(\boldsymbol{R}_{n,m} = 0, \omega)$ that cannot be separated by cutting a single edge (usually called 'irreducible diagrams'), where $G_\sigma(\boldsymbol{R}_{n,m} = 0, \omega)$ is the exact GF of the f-electrons in the real space representation for $n = m$. This property is only valid in the limit $d \to \infty$, so that all the diagrams that are not f.t.p.r have their vertices collapsed until the associated embeddings are f.t.p.r. The exact GF can then be written

$$G_{\mathrm{f},\sigma}(\boldsymbol{k}, \omega) = M_{2,\sigma}^{\mathrm{eff}}(\omega)\frac{1}{1 - |V(k)|^2 G_{\mathrm{c},\sigma}^o(k, \omega)M_{2,\sigma}^{\mathrm{eff}}(\omega)}. \tag{5.1}$$

A practical difficulty in the study of correlated electron systems with cumulant expansions, is that the higher order cumulants rapidly become very laborious to calculate. To consider in some way the higher order cumulants, we are studying the substitution of $M_{2,\sigma}^{\mathrm{eff}}(\omega)$ by an approximate quantity $M_{2,\sigma}^{\mathrm{at}}(\omega)$, derived from an exactly soluble model. To this purpose we use the same PAM but in the atomic limit [20], i.e. when the hopping of the c-electrons is eliminated by taking a conduction band of zero width. This attempt will be discussed in another publication and the present work provides an essential guidance to that study, by showing that all the cumulant diagrams present in $M_{2,\sigma}^{\mathrm{eff}}(\omega)$ are also present in the approximate $M_{2,\sigma}^{\mathrm{at}}(\omega)$. Although the hopping is missing from the $M_{2,\sigma}^{\mathrm{at}}(\omega)$, the exact solution of the conduction band shall appear in the 'hopping between dressed atoms' [12] through the $G_{\mathrm{c},\sigma}^o(k, \omega)$ in equation (5.1).

Appendix A. Separation of vertices

In section 4 it is shown that the contribution of a 'mother' vacuum diagram that is not f.t.p.r. can be estimated from those of several f.t.p.r. 'daughter' diagrams that are derived from the original one. The daughter diagrams are obtained by separating the mother diagram into several f.t.p.r. subdiagrams: a vacuum diagram plus several GF diagrams obtained by adding external lines of the Bose type to the vertices that these separated diagrams have in common with the mother diagram. To show the procedure, it is convenient to analyse a simple case, like that of figure 5(a), and consider only a single vertex in real space, as shown in figure A.1(a), assuming first that it does not belong to the vacuum daughter diagram. Writing only that part P of the total contribution to the mother diagram that have
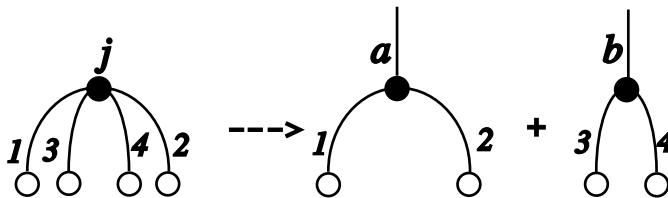

Figure A.1. Separation of a vertex with four edges into a pair of vertices with two edges each.

parameters connected to the particular vertex under consideration, one obtains

$$P = \sum_j \int d1 \int d2 \int d3 \int d4 \sum_{k_1 k_2} \sum_{k_3 k_4} \exp[-i(k_1 - k_2 + k_3 - k_4) \cdot R_j]$$
$$\times V(1)V^*(2)V(3)V^*(4)G_c^0(1)G_c^0(2)G_c^0(3)G_c^0(4)M_4^0(j, 1, 2, 3, 4) \qquad (A.1)$$

where the $G_c^0(s)$ are the c-electron GF, and the other abbreviations are those introduced in section 4. The time or frequency dependence has been left out because it only plays a trivial role in this proof. The corresponding contribution P_a to one daughter diagram for fixed values ℓ_1, ℓ_2 of the internal lines joining the vertex and with an added external line of momentum K_a and parameters ℓ_a is

$$P_a(K_a, \ell_a, \ell_1, \ell_2) = \frac{1}{\sqrt{N}} \sum_{k_1 k_2} \sum_j \exp[-i(k_1 - k_2 + K_a) \cdot R_j]$$
$$\times M_3^0(j, a, 1, 2)V(1)V^*(2)G_c^0(1)G_c^0(2) \qquad (A.2)$$

and the contribution $P_b(K_b, \ell_b, \ell_3, \ell_4)$ of the other daughter diagram is trivially obtained by replacing $a, 1, 2$ by $b, 3, 4$.

Transforming $P_a(K_a, \ell_a, \ell_1, \ell_2)$ to real space, the contribution associated to a site R_j is given by

$$P_a(R_j, \ell_a, \ell_1, \ell_2) = \frac{1}{\sqrt{N}} \sum_{K_a} \exp(iK_a \cdot R_j) P_a(K_a, \ell_a)$$
$$= \sum_{k_1 k_2} \exp[-i(k_1 - k_2) \cdot R_j] V(1)V^*(2)G_c^0(1)G_c^0(2)M_3^0(j, a, 1, 2) \qquad (A.3)$$

and a similar expression $P_b(R_j, \ell_b)$ is obtained for the other daughter diagram. It is clear that the only difference between the product $P_a(R_j, \ell_a, \ell_1, \ell_2)P_b(R_j, \ell_b, \ell_3, \ell_4)$ and the term corresponding to R_j and fixed $\ell_1, \ell_2, \ell_3, \ell_4$ in equation (A1) is given by the cumulants M^0, which are all independent on both R_j and the space dimension d. It then follows that

$$P = \int d1 \int d2 \int d3 \int d4 \frac{M_4^0(j, 1, 2, 3, 4)}{M_3^0(j, a, 1, 2)M_3^0(j, b, 3, 4)}$$
$$\times \sum_j P_a(R_j, \ell_a, \ell_1, \ell_2)P_b(R_j, \ell_b, \ell_3, \ell_4) \qquad (A.4)$$

gives the dependence of P on d.

When one of the two daughter diagrams is chosen as the vacuum one, it is necessary to consider the corresponding contribution

$$\overline{P}(R_j, \ell_1, \ell_2) = \sum_{k_1 k_2} \exp[-i(k_1 - k_2) \cdot R_j] V(1)V^*(2)G_c^0(1)G_c^0(2)M_2^0(j, 1, 2) \qquad (A.5)$$

that was obtained replacing $M_3^0(j, a, 1, 2)$ by $M_2^0(j, 1, 2)$ in equation (A.3): this is the quantity that appears in the corresponding vertex of the vacuum daughter diagram. In this case, instead of equation (A.4) one has the relation

$$P = \int d1 \int d2 \int d3 \int d4 \frac{M_4^0(j, 1, 2, 3, 4)}{M_2^0(j, 1, 2)M_3^0(j, b, 3, 4)}$$
$$\times \sum_j \overline{P}(R_j, \ell_1, \ell_2)P_b(R_j, \ell_b, \ell_3, \ell_4). \qquad (A.6)$$

These are the relations employed in section 4 to prove that only embeddings that are f.t.p.r. give a non-zero contribution, thus leading to the collapse of vertices when they cannot be separated by cutting at most two edges.

Appendix B. Diagrams that are not f.t.p.r.

In the procedure discussed in section 4 a 'mother' vacuum diagram that is not f.t.p.r. is separated into several subdiagrams that have that property. As discussed before, one of the daughter diagrams is chosen as a vacuum diagram, and the remaining ones are GF diagrams obtained by adding external lines of the Bose type to the vertices that these GF diagrams share with other daughter diagrams in the mother diagram. Let us consider one of the GF daughter diagrams in the reciprocal space, with momenta K_υ, indices u_υ and transitions $\alpha_\upsilon(\upsilon = 1, 2, \ldots, n)$ assigned to the $n \geqslant 2$ external vertices, where the α_υ correspond to pair of states with equal number of electrons, i.e. to operators X_α of the Bose type. All these external parameters will be indicated by $\{K_\upsilon, \ell_\upsilon\}$, while $\{\ell\}_{\text{int}}$ will be used for the set of ℓ associated with the internal edges joining all the external vertices. The contribution corresponding to fixed $\{\ell\}_{\text{int}}$ of a split diagram is denoted by $F(\{K_\upsilon, \ell_\upsilon\}, \{\ell\}_{\text{int}})/N^{n/2}$, where the factor $1/\sqrt{N}$, associated to each external line joining an f-vertex (cf [2, Rule 3.7]), has been explicitly written. To transform from K_υ to position variables R_υ one should calculate

$$\overline{F}(\{R_\upsilon\}, \{\ell\}) = (\sqrt{N})^{-n} \sum_{\{K_\upsilon\}} (F(\{K_\upsilon, \ell_\upsilon\}, \{\ell\}_{\text{int}})/N^{n/2}) \exp\left[i \sum_{\upsilon=1}^{n} K_\upsilon \cdot R_\upsilon\right] \tag{B.1}$$

where $\{\ell\}$ denotes all the ℓ, both internal and external. From the translational invariance of the system (or from wavevector conservation at all the vertices) it follows that $\sum_\upsilon K_\upsilon = 0$, so that

$$\overline{F}(\{R_\upsilon\}, \{\ell\}) = \left\{\prod_{\upsilon=1}^{n-1}\left(\frac{1}{N}\sum_{K_\upsilon}\exp[iK_\upsilon(R_\upsilon - R_n)]\right)\right\} F(\{K_\upsilon, \ell_\upsilon\}, \{\ell\}_{\text{int}}). \tag{B.2}$$

In the two hybridization models considered in this work, the external wavevectors K_υ appear in $F(\{K_\upsilon, \ell_\upsilon\}, \{\ell\}_{\text{int}})$ only through the delta that gives the wavevector conservation at each external vertex. The internal wavevectors k appear through the $E_{k,\sigma}$ in $G^o_{c,k\sigma}(\omega)$ (i.e. the c-electron GF of equation (3.8)) and also in the $V_\sigma(k) = -(V_\sigma/t)E_{K,\sigma}$ (cf equation (3.10)) for the n.n. hybridization model. When the wavevector conservation at all vertices is considered explicitly, the number of summations over internal k is reduced, but the arguments of the $E_{k,\sigma}$ become linear combinations of both the remaining external and internal k. To illustrate this result, consider the diagram in figure B.1: applying momentum conservation one can write

$$F(\{K_a, \ell_b, K_a, \ell_a\}, \{\ell_1, \ell_2, \ell_3, \ell_4\}) = \sum_{k_1} M_3^0(b, 1, 2)M_3^0(a, 3, 4)|V_\sigma(k_1)|^2$$

$$\times |V_\sigma(k_1 - K_a)|^2 G^o_{c,\sigma_1}(k_1)G^o_{c,\sigma_2}(k_1 - K_a) \tag{B.3}$$

where the frequencies are not explicitly written because they don't play any role in this analysis. There is only a single summation over k_1, because from the sum over k_2 only $k_2 = k_1 - K_a$ remains.

To study the general case, it is convenient to write (cf equation (2.4))

$$E_{k,\sigma} \equiv E_\sigma(k) = -\sum_{s=1}^{d} \theta_s \cos(ak_s) \tag{B.4}$$

so that $F(\{K_\upsilon, \ell_\upsilon\}, \{\ell\}_{\text{int}})$ can be expanded in a series of the θ_s, putting $\theta_s = \theta = t/\sqrt{2d}$ at the end of the derivation. To analyse the dependence of $\overline{F}(\{R_\upsilon\}, \{\ell\})$ with θ, it is convenient to concentrate first on a given external vertex υ, and write $K_\upsilon = Q = (Q_1, \ldots, Q_d)$ and
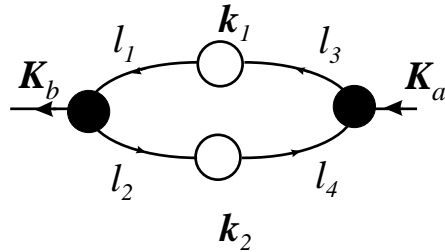
Figure B.1. A simple f.t.p.r diagram. The conservation of moment k at the vertex b gives $k_1 - k_2 - K_b = 0$ for $u_b = -1$ and that at vertex a gives $k_2 - k_1 + K_a = 0$ for $u_a = +1$, so that $K_a = K_b$ as should be expected from the translational invariance of the system. Only one summation over k_1 remains because $k_2 = k_1 - K_a$.

$R_\upsilon - R_n = R = (R_1, \ldots, R_d)$. Equation (B.2) shows that for a given external vertex υ, there is a $\sum_{Q_s} \exp(\mathrm{i} Q_s R_s)$ applied to $F(\{K_\upsilon, \ell_\upsilon\}, \{\ell\}_{\mathrm{int}})$ for each dimension $s = 1, \ldots, d$ of the space, and when for a given s it is $R_s \neq 0$, all the terms independent of θ_s in the expansion of $F(\{K_\upsilon, \ell_\upsilon\}, \{\ell\}_{\mathrm{int}})$ will cancel out (cf equation (3.17)). It then follows that $\overline{F}(\{R_\upsilon\}, \{\ell\}) = \mathrm{O}|\theta^p|$, where $p \geqslant p^0$ and p^0 is the number of dimensions for which there are non-zero components s for at least one of the $n - 1$ vectors $R_\upsilon - R_n$. One can then conclude that unless all the R_υ coincide, the $\overline{F}(\{R_\upsilon\}, \{\ell\})$ is at least of $\mathrm{O}|\theta|$ and it vanishes when $d \to \infty$. This property was used to prove the collapse of vertices discussed in section 4 for diagrams that are not f.t.p.r.

References

[1] Hewson A C 1993 *The Kondo Problem to Heavy Fermions* (Cambridge: Cambridge University Press)
Schlottmann P 1989 *Phys. Rep.* **181** 1
Fulde P 1988 *Solid State Phys.* **41** 1
[2] Figueira M S, Foglio M E and Martinez G G 1994 *Phys. Rev.* B **50** 17 933
[3] Hubbard J 1966 *Proc. R. Soc.* A **296** 82
[4] Hubbard J 1964 *Proc. R. Soc.* A **276** 238
Hubbard J 1964 *Proc. R. Soc.* A **277** 237
Hubbard J 1964 *Proc. R. Soc.* A **281** 401
[5] Wortis M 1974 *Phase Transitions and Critical Phenomena* vol 3 ed C Domb and M S Green (London: Academic) p 113
[6] Metzner W and Vollhardt D 1989 *Phys. Rev. Lett.* **62** 324
[7] Georges A, Kotliar G, Krauth W and Rozenberg M J 1996 *Rev. Mod. Phys.* **68** 13
[8] Jarrel M, Akhlaghpour H and Pruschke Th 1993 *Phys. Rev. Lett.* **70** 1670
Jarrel M 1995 *Phys. Rev.* B **51** 7429
[9] Mutou T and Hirashima D S 1994 *J. Phys. Soc. Japan* **63** 4475
Mutou T and Hirashima D S 1995 *J. Phys. Soc. Japan* **64** 4799
[10] Mutou T and Hirashima D S 1996 *J. Phys. Soc. Japan* **65** 369
[11] Saso T and Itoh M 1996 *Phys. Rev.* B **53** 6877
[12] Metzner W 1991 *Phys. Rev.* B **43** 8549
[13] Tsung-han Lin and Falicov L M 1980 *Phys. Rev.* B **22** 857
[14] Muller Hartmann E 1989 *Z. Phys.* B **74** 507
[15] Figueira M S and Foglio M E 1996 *J. Phys.: Condens. Matter* **8** 5017
[16] Hewson A C 1977 *J. Phys. C: Solid State Phys.* **10** 4973
[17] Yang D H Y and Wang Y L 1975 *Phys. Rev.* B **10** 4714
[18] Metzner W and Vollhardt D 1990 *Helv. Phys. Acta* **63** 364
[19] Craco L and Gusmão M A 1996 *Phys. Rev.* B **54** 1629
[20] Foglio M E and Falicov L M 1979 *Phys. Rev.* B **20** 4554